

Insight into the structural and magnetotransport properties of epitaxial α -Fe₂O₃/Pt(111) heterostructures: Role of the reversed layer sequence

A. Koziol-Rachwał^{1,*}, N. Kwiatek², W. Skowroński³, K. Grochot^{1,3}, J. Kanak³, E. Madej²,
K. Freindl², J. Korecki², and N. Spiridis²

¹Faculty of Physics and Applied Computer Science, AGH University of Science and Technology,
Mickiewicza 30, 30-059 Kraków, Poland

²Jerzy Haber Institute of Catalysis and Surface Chemistry, Polish Academy of Sciences, 30-239 Kraków, Poland

³Institute of Electronics, AGH University of Science and Technology, Mickiewicza 30, 30-059 Kraków, Poland



(Received 8 April 2022; accepted 19 August 2022; published 19 September 2022)

We report on the chemical structure and spin Hall magnetoresistance (SMR) in epitaxial α -Fe₂O₃(hematite)(0001)/Pt(111) bilayers with hematite thicknesses of 6 and 15 nm grown by molecular beam epitaxy on a MgO(111) substrate. Unlike previous studies that involved Pt overlayers on hematite, the present hematite films were grown on a stable Pt buffer layer and displayed structural changes as a function of thickness. These structural differences (the presence of a ferrimagnetic phase in the thinner film) significantly affected the magnetotransport properties of the bilayers. We observed a sign change of the SMR from positive to negative when the thickness of the hematite increased from 6 to 15 nm. For α -Fe₂O₃(15 nm)/Pt, we demonstrated room-temperature switching of the Néel order with rectangular, nondecaying switching characteristics. Such structures open the way to extending magnetotransport studies to more complex systems with double asymmetric metal/hematite/Pt interfaces.

DOI: [10.1103/PhysRevB.106.104419](https://doi.org/10.1103/PhysRevB.106.104419)

I. INTRODUCTION

Spintronic devices based on antiferromagnets (AFMs) offer a wide range of unique properties, such as robustness against magnetic field perturbations, fast spin dynamics, and lack of stray fields [1]. However, the absence of a net magnetic moment in AFM materials is a challenge for electrical reading of their magnetic state, particularly when the AFM layer is insulating. In the last decade, spin Hall magnetoresistance (SMR) [2] was used to probe the direction of spins in insulating AFMs in contact with a metal characterized by a finite spin Hall angle. The SMR effect, characterized by the dependence of the resistance of the metallic thin film with strong spin-orbit coupling on the direction of the magnetization orientation of the adjacent magnetic layer, was first demonstrated in collinear ferrimagnet/heavy metal (HM) bilayers [3–8] and applied to ferromagnet (FM)/HM structures [9]. The SMR effect manifests itself as sinusoidal oscillations of the Pt resistance in response to rotation of the ferrimagnet magnetization induced by an external magnetic field. For canted and spiral ferrimagnets (Gd₃Fe₅O and Cu₂OSeO₃, respectively), the SMR was used to identify noncollinear magnetic phases [10,11]. More recently, the SMR was reported in heterostruc-

tures comprising AFMs. Shang *et al.* investigated how the proximity of NiO with different thicknesses influences the SMR signal in the Pt/NiO/Y₃Fe₅O₁₂ stack. Calculations performed for the AFM/HM bilayer showed that the SMR can be used to determine the magnetic anisotropy and the Néel order in the AFM layer [12], for which, despite the absence of net magnetization, a nonzero SMR arises, which is an effect of the individual interaction of magnetic sublattices with the spin current. SMR in the AFM/HM bilayer was experimentally shown for Ta/Cr₂O₃ [13] and Pt/NiO [14–16]. For AFMs, a 90° phase shift (so-called “negative” SMR) was observed compared to the SMR observed in ferrimagnet/Pt bilayers (known as “positive” SMR) due to the orthogonal alignment of the AFM spins with respect to the external magnetic field exceeding the spin-flop field [16]. Most recently, negative SMR was presented for another HM/AFM bilayer, Pt/ α -Fe₂O₃ [17,18]. Importantly, the presence of small net magnetization in α -Fe₂O₃ layers enabled the magnetotransport properties of α -Fe₂O₃ in a relatively small magnetic field to be revealed. Fischer *et al.* [17] noted sinusoidal oscillations of the Pt resistivity together with rotation of the Néel vector of the α -Fe₂O₃ layer, with the amplitude of the SMR signal three times higher than that observed for the Pt/NiO system. In parallel, Cheng *et al.* demonstrated electrical switching of tristate Néel order in Pt/ α -Fe₂O₃ bilayers by measuring the Hall resistance [18]. Reversible and repeatable switching of the spin structure induced by electric current pulses was confirmed by direct observation of the domain structure with the use of a photoemission electron microscope [19]. These results, together with a recent theoretical and experimental demonstration of spin-pumping signals, inverse spin-Hall voltages

*akoziol@agh.edu.pl

[20,21], and long-distance spin transport in hematite [22,23], indicate that the Pt/ α -Fe₂O₃ system has strong potential for antiferromagnetic spintronic applications.

In previous experimental studies concerning the magnetotransport properties of Pt/ α -Fe₂O₃, hematite layers with thicknesses of a few tens of nanometers were grown by sputtering [18,19,24] or pulsed laser deposition [17] on Al₂O₃(0001) single crystals, followed by *in situ* room-temperature deposition of thin Pt films. Whereas room-temperature deposition of the Pt layer prevents reduction of the AFM hematite layer to ferrimagnetic magnetite (Fe₃O₄) [25,26], the nonannealed Pt layer is structurally unstable, which can affect the magnetotransport properties of the Pt/ α -Fe₂O₃ bilayer. In particular, Cheng *et al.* [18] reported current-induced triangular-shaped Hall resistance changes in the as-grown Pt/ α -Fe₂O₃ bilayer grown by sputtering. They showed that triangular switching is an artifact that can be attributed to the current-driven migration of grain boundaries in the Pt layer and is not related to AFM switching, which confirms previous theoretical and experimental studies [27]. Interestingly, annealing of the sample by high current pulses was shown to result in single-pulse saturated, steplike switching of the AFM and improve the Pt stability. Notably, the postdeposition treatment temperature can influence the Pt/ α -Fe₂O₃ interface, which is crucial for magnetotransport effects. Cheng *et al.* showed that interdiffusion of Fe and Pt at the Pt/ α -Fe₂O₃ interface can lead to the formation of FePt alloy and induction of magnetization in Pt, which affects the magnetotransport properties of the system at low temperature [24].

To dispel doubts about the stability of the Pt/ α -Fe₂O₃ interface and its changes induced by annealing, a reversed α -Fe₂O₃/Pt structure can be considered. The use of the Pt layer as the substrate enables its deposition at elevated temperature and/or postdeposition annealing prior to the growth of α -Fe₂O₃, which provides the formation of a stable α -Fe₂O₃/Pt interface.

In our studies, we investigated the chemical and magnetotransport properties in the epitaxial α -Fe₂O₃/Pt structure, where hematite α -Fe₂O₃(0001) thin films with thicknesses of (6 ± 0.3) nm and (15 ± 0.5) nm were grown on a 7 nm thick epitaxial Pt(111) layer on MgO(111). Whereas surface-sensitive methods indicated only the hematite phase, Mössbauer spectroscopy measurements showed that the bulk-like hematite phase contributed 96% and 66% of the total spectral intensity for the thicker and thinner oxide layers, respectively. Although the thinner film contains almost a one-third contribution from a spinel phase, for simplicity, we refer to the thinner and thicker samples as α -Fe₂O₃(6)/Pt and α -Fe₂O₃(15)/Pt, respectively. An SMR study revealed that the chemical structure determines the magnetotransport properties of the α -Fe₂O₃/Pt bilayer. We noted a sign change of the SMR from positive to negative when the thickness of the oxide was increased, which was discussed in terms of the residual ferrimagnetic phase present in the thinner layer. Finally, for α -Fe₂O₃(15)/Pt, we demonstrated electrical switching. For the as-grown sample, we registered steplike, nondecaying switching between three antiferromagnetic order states, which demonstrates the stability of the interface in our samples.

II. STRUCTURAL AND MAGNETIC CHARACTERIZATION

Hematite (α -Fe₂O₃), which is the most stable phase of iron oxide, crystallizes in the trigonal corundum structure with a hexagonal unit cell. Above the Morin transition temperature ($T_M = 250$ K) [28] and below the Néel temperature ($T_N = 953$ K) [28], the spins of the Fe³⁺ ions are ferromagnetically aligned within the (0001) plane, whereas neighboring (0001) planes form “ABBA” stacking along the [0001] direction (*c* axis). For $T_M < T < T_N$, the Dzyaloshinskii-Moriya interaction (DMI) induces slight canting of two AFM sublattices, which leads to the appearance of a weak ferromagnetism, with the ferromagnetic component almost perpendicular to one of the three easy axes, i.e., [10 $\bar{1}$ 0], [0 $\bar{1}$ 10], and [$\bar{1}$ 100] within the (0001) plane [29]. Below T_M , hematite undergoes a transition to an easy-axis AFM with spins antiferromagnetically aligned along the *c* axis [30]. In thin films, with the decrease in hematite thickness, a decrease in T_M or complete disappearance of the transition was observed. The transition was also shown to be restorable by doping [31–33].

In our study, α -Fe₂O₃/Pt bilayers were prepared in a multichamber UHV system. A one side polished MgO(111) single crystal was used as the substrate. Prior to deposition, the substrate was degassed for 30 min at 870 K. A 7 nm thick epitaxial Pt(111) layer was deposited at a rate of 0.06 nm/min at room temperature and annealed at 800 K for 30 min to improve its surface quality. Hematite layers were grown via oxidation of magnetite Fe₃O₄(111) films [27]. First, magnetite layers were grown by reactive deposition of Fe in a molecular oxygen atmosphere under a partial pressure of 8×10^{-6} mbar and a substrate temperature of 523 K. The samples were prepared with the use of the ⁵⁷Fe isotope to enable Mössbauer spectroscopy studies. After deposition of 3 nm of metallic Fe (which corresponds to 6.3 nm of Fe₃O₄), half of the sample was protected by a shutter, while the deposition of Fe was continued on the uncovered part of the sample up to 7 nm (which corresponds to 14.7 nm of Fe₃O₄). As a result, two regions with different magnetite thicknesses were formed on the sample. Following Fe₃O₄ deposition, the sample was annealed at 770 K for 30 min. Oxidation of magnetite to hematite was performed by exposition of the Fe₃O₄ layers to oxygen, up to a total dose of 6075 l (2700 s at an oxygen partial pressure of 3×10^{-5} mbar) while the substrate was kept at 770 K. The corresponding nominal thickness d_h of the hematite films was 6.4 and 14.9 nm, with a thickness uncertainty of approximately ±5% (the accuracy of the deposition rate determination based on a quartz crystal monitor) and, for simplicity, hereafter the hematite thicknesses are referred to as 6 and 15 nm, respectively. After each preparation step, the films were characterized *in situ* by low energy electron diffraction (LEED). Additionally, at selected growth stages, analogous samples were characterized by scanning tunneling microscopy (STM) (see Supplemental Material [34]). LEED patterns collected for the Pt, Fe₃O₄ and α -Fe₂O₃ surfaces revealed epitaxial growth of the layers and confirmed the formation of an α -Fe₂O₃/Pt bilayer with the epitaxial relation α -Fe₂O₃[2 $\bar{1}$ $\bar{1}$ 0]||Pt[10 $\bar{1}$]||MgO[10 $\bar{1}$] (Supplemental Material, Fig. S1 [34] and Refs. [1–3,5] in the Supplemental Material). From the surface-sensitive methods

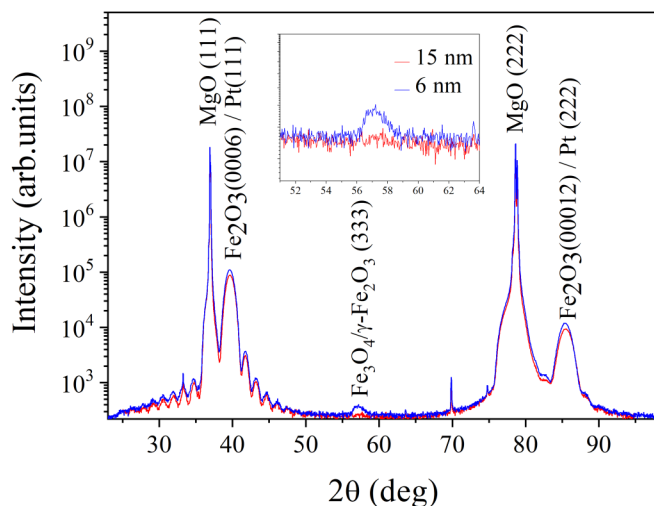


FIG. 1. XRD patterns of α -Fe₂O₃/Pt/MgO(111) with hematite layer thicknesses of 6 nm (blue) and 15 nm (red).

LEED and STM, no phases other than hematite could be confirmed. Figure 1 shows $2\theta/\omega$ x-ray diffraction (XRD) scans of α -Fe₂O₃/Pt/MgO(111) for hematite thicknesses of 6 nm (blue) and 15 nm (red). For both parts of the sample, we observed reflections from the MgO substrate and interference of reflections from α -Fe₂O₃(0001) and Pt(111) layers. Interestingly, for the thinner hematite film, we noted an additional peak at a 2θ of approximately 57° , which can be a feature of the residual spinel structure in the oxide layer [35]. To unambiguously resolve the composition of the iron oxide films, we used conversion electron Mössbauer spectroscopy (CEMS). The undisputed advantages of MS, such as sensitivity to different chemical and structural atomic positions, make the method a perfect tool for characterization of iron oxides [36,26]. The Mössbauer spectra of iron oxides with a long-range magnetic order are magnetically split and possess a characteristic set of hyperfine parameters, i.e., isomer shift (IS), quadrupole splitting (QS), and hyperfine magnetic field (B_{HF}). Thus, numerical analysis of the spectrum allows identification and quantification of iron oxides. Particularly, a distinct feature of hematite is a pronounced quadrupole

interaction that is present in compounds with trigonal symmetry, such as hematite, and almost vanishes for spinel cubic structures, such as magnetite or maghemite.

Figures 2(a) and 2(b) show room-temperature CEMS spectra collected for the 6 and 15 nm films, respectively (for measurement details and fitting parameters, see Supplemental Material, Table I [34] and Ref. [7] in the Supplemental Material). Both spectra are dominated by six line components (magenta shaded regions) with $QS = -0.11$ mm/s, $IS = 0.37$ mm/s, and an average hyperfine magnetic field B_{HF} of 50.9 and 51.7 T for the thinner and thicker layers, respectively, which unambiguously identifies regular Fe³⁺ sites in the corundum structure of hematite [26]. These components possess a bimodal B_{HF} distribution, where the low intensity broader subcomponents with lower B_{HF} (darker shaded regions in Fig. 2) represent surface hematite layers [25]. Additionally, the more complex spectrum for the 6 nm film exhibits a 30% contribution of sites [green shaded component in Fig. 2(a)] whose hyperfine parameters, in particular $IS = 0.26$ mm/s and $QS = 0.03$ mm/s, are close to those of a spinel phase, namely, maghemite (γ -Fe₂O₃). The spinel phase (maghemite or nonstoichiometric magnetite, whose Mössbauer sextets are indistinguishable [37]) is a natural residue of the precursor phase for hematite that is obtained via oxidation of magnetite. The epitaxially stabilized spinel phase is more likely to occur in the thinner 6 nm layer than in the 15 nm film, as the stabilization of the spinel/hematite bilayer for the latter case would incur a much higher strain energy. A similar tendency was also found during direct growth of iron oxide films on Pt(111), where the early stages of growth favor maghemite and the thermodynamically stable phase, hematite, is stabilized in the thicker layer regime [26]. The broad distribution of B_{HF} for this component is an interfacial effect previously reported in systematic studies of the oxidation of magnetite to hematite [26]. From line intensities in the spectra in Fig. 2 that were measured with the gamma rays along the film normal it is clear that the AFM spins lay in the (0001) plane, as expected for hematite above the Morin temperature. Additional measurements at the grazing incidence as a function of the azimuthal angle indicate the threefold symmetry of the in-plane spin distribution corresponding to the three easy axes (see Supplemental Material for details [34]).

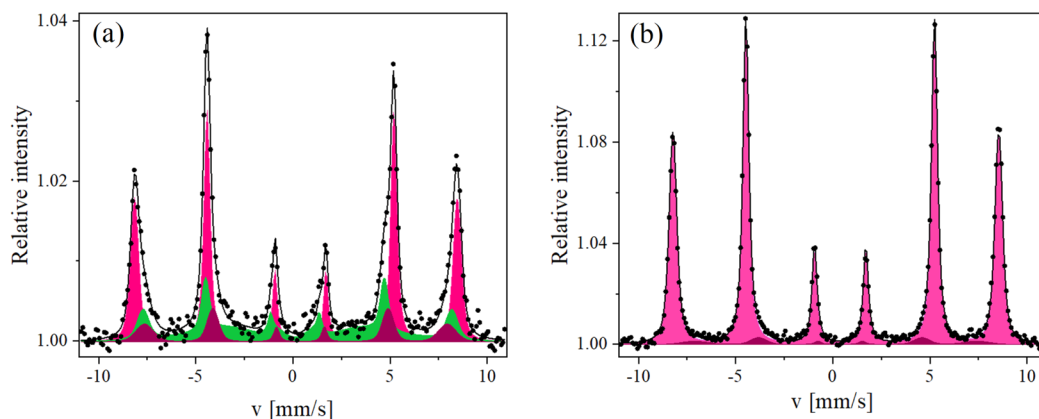


FIG. 2. Experimental CEMS spectra (points) of α -Fe₂O₃/Pt, and results of the best fits (lines) and their deconvolution into spectral components (shaded) for the 6 nm (a) and 15 nm (b) films. For the color code, see the text.

Notably, down to the temperature of 110 K, we did not observe the Morin transition for either film (which, in the bulk, occurs at a temperature of approximately 250 K). The absence of the Morin transition in thin hematite films was previously reported for α -Fe₂O₃ grown on Pt(111) [26] and Al₂O₃(001) [38] substrates. To summarize, whereas the 15 nm film is fully composed of antiferromagnetic hematite, in the 6 nm film, a 33% contribution of a ferrimagnetic spinel phase must be considered. Comparison of the volume-sensitive methods (XRD and CEMS) with LEED indicates that the spinel phase is localized in deeper layers. The presence of this nonhematite phase can be substantial for the magnetotransport properties of the α -Fe₂O₃/Pt bilayer, as discussed below.

III. SMR MEASUREMENTS

For the magnetotransport experiments, we patterned Hall bar mesa structures on our sample with the use of photolithography and ion beam milling. The width and length of the Hall bars were 30 and 80 μ m, respectively. Room-temperature magnetoresistance measurements were performed by rotating the external magnetic field \mathbf{H}_α relative to the $[\bar{1}100]$ axis of α -Fe₂O₃ within the (0001) plane [Fig. 3(a)]. The SMR measurements were performed as a function of magnetic field strength. Longitudinal resistances (R_{xx}) were determined from four-wire resistance measurements in which a dc current density of 9.2×10^{10} A/m² (J_c) was applied along the $[\bar{1}100]$ crystal axis of α -Fe₂O₃ (x axis) (see Supplemental Material for details of the measurements [34]). Figure 3 shows the $R_{xx}(\alpha)$ dependence obtained for the α -Fe₂O₃/Pt bilayers with hematite thicknesses of 15 nm [Fig. 3(b)] and 6 nm [Fig. 3(c)]. For both hematite thicknesses, we noted SMR oscillations with a period of 180°. Interestingly, we observed a phase shift of 90° in the $R_{xx}(\alpha)$ dependences measured for the d_h of the 6 and 15 nm bilayers. Whereas for the thinner film, we noted R_{xx} maxima for \mathbf{H}_α parallel/antiparallel to the x direction and longitudinal resistance minima for \mathbf{H}_α perpendicular to x (parallel/antiparallel to the y direction), the R_{xx} maxima and minima for $d_h = 15$ nm appear for $\mathbf{H}_\alpha \parallel \pm y$ and $\mathbf{H}_\alpha \parallel \pm x$, respectively. The $R_{xx}(\alpha)$ characteristic observed for the thicker hematite layer [Fig. 3(b)] results from the perpendicular alignment of the Néel vector with respect to the external magnetic field and is a fingerprint of AFM SMR (so-called negative SMR) [16]. The amplitude of the AFM SMR obtained in our study for α -Fe₂O₃(15)/Pt(7) saturates at a magnetic field of 2 T (Fig. S3, Supplemental Material [34]), similarly to the previous studies obtained for reversed Pt/ α -Fe₂O₃ structure [17]. At 2 T the amplitude of the SMR is approximately 1×10^{-4} . This value is higher than the SMR amplitude noted for the Pt(3.5)/NiO(120) bilayer registered at a magnetic field of 15 T [16]. For our thinner film, we noted a 90° phase shift in the SMR signal [Fig. 3(c)]; i.e., the SMR exhibits the $\cos^2\alpha$ dependence expected for FM/HM bilayers (positive SMR), in which the FM magnetization aligns parallel to \mathbf{H}_α [2]. A positive SMR has been recently reported for AFMs, and its origin was attributed to the presence of either a ferromagnetic component at the AFM/HM interface or a canted AFM spin structure [13,39–42]. For bulk hematite, the small net magnetization induced by the DMI was shown to not contribute to the

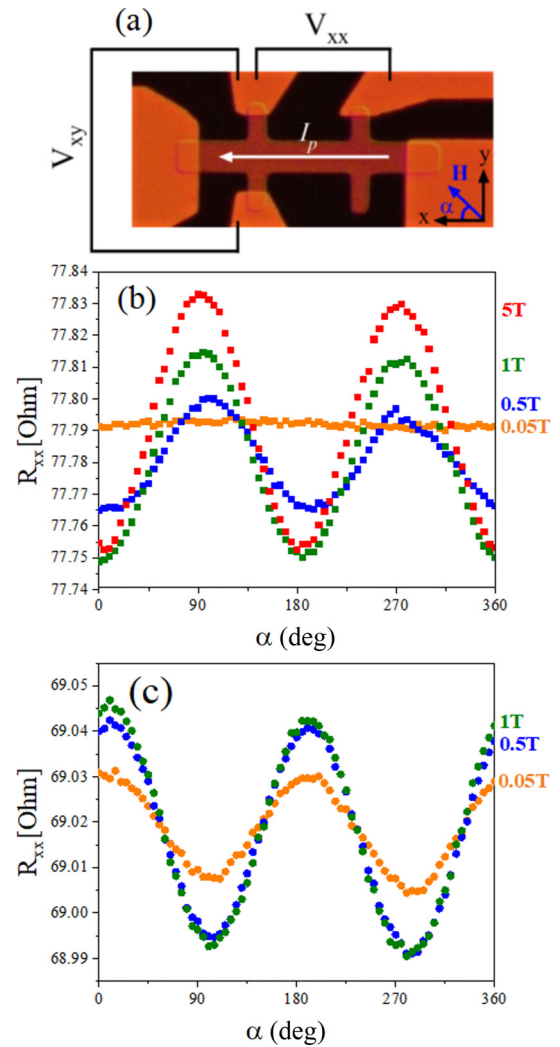


FIG. 3. (a) Schematic of the Hall bar structure prepared for α -Fe₂O₃/Pt bilayers. During the SMR measurements, the external magnetic field was rotated in the α -Fe₂O₃ (0001) plane (xy plane) relative to the $[\bar{1}100]$ axis of α -Fe₂O₃ (x axis). (b), (c) Longitudinal SMR, respectively, for α -Fe₂O₃(15)/Pt(7) and α -Fe₂O₃(6)/Pt(7) performed for different strengths of magnetic field.

electrical response, which is dominated by the AFM Néel vector [43]. Thus, a negative SMR is expected for α -Fe₂O₃/Pt bilayers, as we found for the thicker hematite layer. In our study, the appearance of a positive SMR for the α -Fe₂O₃(6)/Pt bilayer is associated with a notable contribution of a spinel-like component detected in the Mössbauer spectrum, which we localize at the Pt/iron oxide interface. Both Fe₃O₄ and γ -Fe₂O₃ are ferrimagnets and can contribute to the positive SMR. The amplitude of the positive SMR obtained in our study for α -Fe₂O₃(6)/Pt is three times greater than that obtained for Pt(7)/Fe₃O₄(20)/MgO(001) [5] and twice as large as that obtained for the γ -Fe₂O₃/Pt bilayer [44].

The SMR signal appears in the thinner α -Fe₂O₃ sample for much weaker magnetic fields; i.e., we noted clear oscillations of resistance for α -Fe₂O₃(6) at 0.05 T while at the same magnetic field no SMR was noted for α -Fe₂O₃(15) [compare

orange in Figs. 3(b) and 3(c)]. This confirms a higher sensitivity of the ferrimagnetic moment of α -Fe₂O₃(6) to the external magnetic field. Amplitudes of SMR at considerable magnetic fields (see Fig. S3 in the Supplemental Material [34]) are comparable. This suggests that the effectiveness of the spin transfer from the Pt layer to the α -Fe₂O₃(6) and α -Fe₂O₃(15) layers is similar. This result may not be surprising if we consider that both materials consist of Fe³⁺ insulating oxide.

To exclude the proximity-induced anisotropic magnetoresistance (AMR) contribution to the magnetoresistance in our samples we performed additional magnetoresistance measurements in which we rotated the external magnetic field within the plane perpendicular to the y direction (xz plane) [5]. For both α -Fe₂O₃(6)/Pt and α -Fe₂O₃(15)/Pt heterostructures we did not observe any oscillation of magnetoresistance within the xz plane characteristic for AMR (Fig. S4 in the Supplemental Material [34]) [5]. Thus, proximity-induced AMR does not contribute to the magnetoresistance in our study.

IV. CURRENT-INDUCED SWITCHING OF THE NÉEL ORDER IN α -Fe₂O₃(15)/Pt(7 nm)

To demonstrate the possibility of current-induced switching between the three easy axes of an AFM α -Fe₂O₃ layer, we patterned the α -Fe₂O₃(15)/Pt(7) bilayer into eight terminal Hall crosses [Fig. 4(a)] in addition to the Hall bar described in the previous section. Three (10 μ m wide) of four electrical paths were aligned along the easy axes of the α -Fe₂O₃ layer, i.e., along [10 $\bar{1}$ 0], [$\bar{1}$ 100], and [0 $\bar{1}$ 10] [black, green, and red arrows in Fig. 4(a), respectively], whereas the fourth path (5 μ m wide) was used to measure the Hall voltage [horizontal path, y direction in Fig. 4(a)]. During the measurements, we used the following switching protocol. A set of 20 1 ms long current pulses (I_p) was applied along one of the easy hematite directions. After a 1 s delay, a reading current of 0.18 mA was applied along the [$\bar{1}$ 100] axis, and the transversal Hall voltage (V_H) was recorded. This series was repeated 15 times. Then, the series of current pulses were applied along the other easy axes. Figure 4(b) presents the change in the transverse resistance (ΔR_{xy}) as a function of the number of current pulses for different current densities j . Similar to a previous study performed for the reversed Pt/ α -Fe₂O₃ structure [18], we observed a tristate Hall resistance after the application of the series of current pulses along the three easy axes of hematite. According to previous theoretical and experimental studies, a pulse current applied along one of the easy axes of an AFM exerts a spin-orbit torque (SOT) on the Néel order parameter and aligns it parallel to I_p [18]. Application of current pulses along the [10 $\bar{1}$ 0], [$\bar{1}$ 100], and [0 $\bar{1}$ 10] axes results in stabilization of the high, intermediate, and low R_{xy} states, respectively. To confirm the direction of the Néel vector (\mathbf{L}) corresponding to a given resistance state, we determined the transverse Hall resistance (R_{xy}) dependence on the α angle at an in-plane magnetic field of 0.8 T [Fig. 3(a)]. Due to the spin flop, at $\alpha = -30^\circ$, the Néel vector is aligned along the [0 $\bar{1}$ 10] axis, whereas for $\alpha = 30^\circ$ and $\alpha = 90^\circ$, the spins of hematite are parallel and antiparallel to [10 $\bar{1}$ 0] and [$\bar{1}$ 100], respectively. The dependence of R_{xy} on α confirms that the state with the highest resistance is obtained for $\mathbf{L}||$ [10 $\bar{1}$ 0]

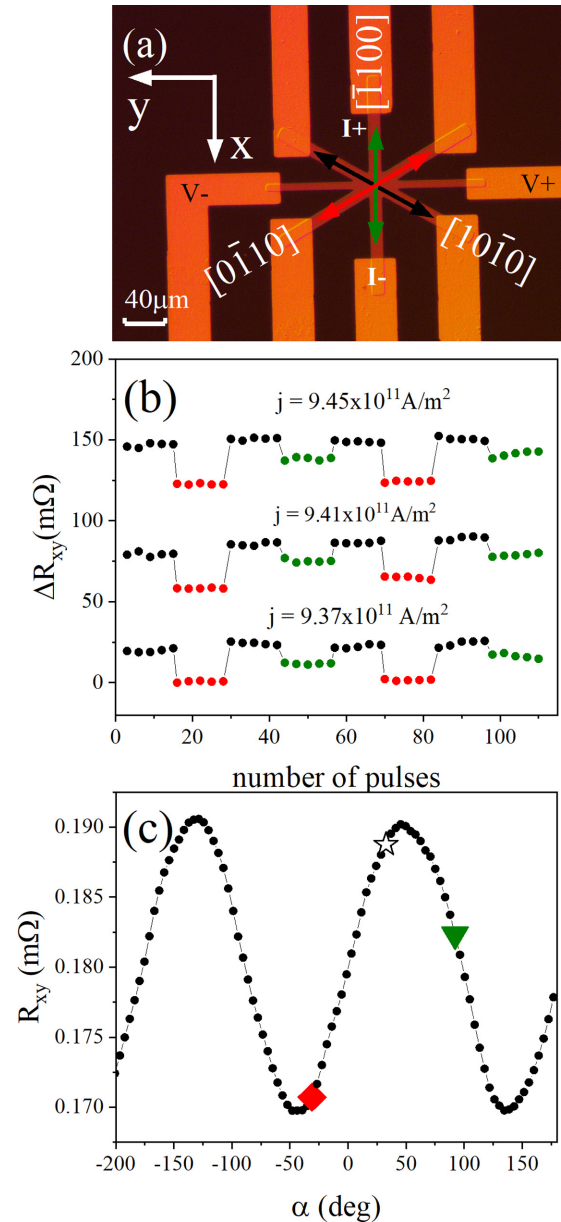


FIG. 4. (a) Optical microscopy image of the eight-terminal device used for the Néel order switching experiment on the α -Fe₂O₃(15 nm)/Pt bilayers. (b) Change in the transverse resistance as a function of the number of current pulses applied along the three easy axes of hematite. Measurements with different j are artificially offset for clarity. (c) Dependence of the transversal resistivity (R_{xy}) on angle α at $\mathbf{H}_\alpha = 0.8$ T.

[Fig. 4(c), empty star], whereas the intermediate and lowest transverse resistances are generated for $\mathbf{L}||$ [$\bar{1}$ 100] [Fig. 4(c), green triangle] and $\mathbf{L}||$ [0 $\bar{1}$ 10] [Fig. 4(c), red square], respectively. In agreement with the theory of a dampinglike SOT [45], together with an increase in the current density, we noted an increase in ΔR_{xy} from 19 to 26 m Ω when j changed from 9.37×10^{11} A/m² to 9.45×10^{11} A/m². The current densities required for reorientation of the Néel vector are similar to the values reported for magnetization switching in FM/HM multilayers [46,47]. Importantly, in our experiment, we noted rectangular, nondecaying switching characteristics with no

traces of sawtooth features for the as-grown sample. This result is distinct from switching experiments performed for the reversed Pt/ α -Fe₂O₃ structure, for which sawtooth-shaped switching of ΔR_{xy} was observed for the as-prepared sample and steplike switching appeared only after annealing of the sample with high current pulses [18]. We attribute this difference to the stable α -Fe₂O₃/Pt interface formed during the growth of our sample, which remained unaffected by the current pulse treatment.

V. SUMMARY AND CONCLUSIONS

We investigated the structure and magnetotransport properties of α -Fe₂O₃/Pt bilayers with two iron oxide thicknesses, 6 and 15 nm. Mössbauer spectroscopy measurements showed that the hematite phase dominates for both oxide thicknesses; however, for the thinner film, interfacial contributions of a residual spinel structure are notable. The structural difference affects the magnetotransport properties of the α -Fe₂O₃/Pt bilayers. Whereas for the thicker film, we observed a negative SMR, which is characteristic of AFM/HM bilayers, the sign of the SMR for the bilayer with the thinner oxide film was positive. We attributed the change in the SMR sign to the interfacial ferrimagnetic order within the spinel phase.

Finally, for α -Fe₂O₃(15)/Pt, we demonstrated room-temperature switching of the Néel vector. The steplike nondecaying switching observed for the as-grown sample reveals the formation of a stable AFM/HM interface in our samples. We also note that such structures, with hematite grown on Pt, open the way to extending magnetotransport studies to more complex systems with double asymmetric HM/hematite/Pt interfaces.

ACKNOWLEDGMENTS

This work was supported by Grant No. 2016/21/B/ST3/00861 funded by the National Science Centre, Poland. A.K.-R. acknowledges Grant No. 2020/38/E/ST3/00086 funded by the National Science Centre, Poland. J.K and K.F acknowledge Grant No. 2020/39/B/ST5/01838 funded by the National Science Centre, Poland. W.S. acknowledges Bekker Grant No. PPN/BEK/2020/1/00118/DEC/1 from the Polish National Agency for Academic Exchange. The authors acknowledge Felix Casanova and Luis Hueso for their technical expertise in the magnetotransport measurement.

-
- [1] M. B. Jungfleisch, W. Zhang, and A. Hoffmann, Perspectives of antiferromagnetic spintronics, *Phys. Lett. A* **382**, 865 (2018).
- [2] Y. T. Chen, S. Takahashi, H. Nakayama, M. Althammer, S. T. B. Goennenwein, E. Saitoh, and G. E. W. Bauer, Theory of spin Hall magnetoresistance, *Phys. Rev. B* **87**, 144411 (2013).
- [3] H. Nakayama, M. Althammer, Y.-T. Chen, K. Uchida, Y. Kajiwara, D. Kikuchi, T. Ohtani, S. Geprägs, M. Opel, S. Takahashi, R. Gross, G. E. W. Bauer, S. T. B. Goennenwein, and E. Saitoh, Spin Hall Magnetoresistance Induced by a Nonequilibrium Proximity Effect, *Phys. Rev. Lett.* **110**, 206601 (2013).
- [4] N. Vlietstra, J. Shan, V. Castel, B. J. van Wees, and J. Ben Youssef, Spin-Hall magnetoresistance in platinum on yttrium iron garnet: Dependence on platinum thickness and in-plane/out-of-plane magnetization, *Phys. Rev. B* **87**, 184421 (2013).
- [5] M. Althammer, S. Meyer, H. Nakayama, M. Schreier, S. Altmannshofer, M. Weiler, H. Huebl, S. Geprägs, M. Opel, R. Gross, D. Meier, C. Klewe, T. Kuschel, J.-M. Schmalhorst, G. Reiss, L. Shen, A. Gupta, Y.-T. Chen, G. E. W. Bauer, E. Saitoh *et al.*, Quantitative study of the spin Hall magnetoresistance in ferromagnetic insulator/normal metal hybrids, *Phys. Rev. B* **87**, 224401 (2013).
- [6] C. Hahn, G. de Loubens, O. Klein, M. Viret, V. V. Naletov, and J. Ben Youssef, Comparative measurements of inverse spin Hall effects and magnetoresistance in YIG/Pt and YIG/Ta, *Phys. Rev. B* **87**, 174417 (2013).
- [7] S. R. Marmion, M. Ali, M. McLaren, D. A. Williams, and B. J. Hickey, Temperature dependence of spin Hall magnetoresistance in thin YIG/Pt films, *Phys. Rev. B* **89**, 220404(R) (2014).
- [8] S. Meyer, M. Althammer, S. Geprägs, M. Opel, R. Gross, and S. T. B. Goennenwein, Temperature dependent spin transport properties of platinum inferred from spin Hall magnetoresistance measurements, *Appl. Phys. Lett.* **104**, 242411 (2014).
- [9] C. O. Avci, K. Garello, J. Mendil, A. Ghosh, N. Blasakis, M. Gabureac, M. Trassin, M. Fiebig, and P. Gambardella, Magnetoresistance of heavy and light metal/ferromagnet bilayers, *Appl. Phys. Lett.* **107**, 192405 (2015).
- [10] K. Ganzhorn, J. Barker, R. Schlitz, B. A. Piot, K. Ollefs, F. Guillou, F. Wilhelm, A. Rogalev, M. Opel, M. Althammer, S. Geprägs, H. Huebl, R. Gross, G. E. W. Bauer, and S. T. B. Goennenwein, Spin Hall magnetoresistance in a canted ferrimagnet, *Phys. Rev. B* **94**, 094401 (2016).
- [11] A. Aqeel, N. Vlietstra, A. Roy, M. Mostovoy, B. J. van Wees, and T. T. M. Palstra, Electrical detection of spiral spin structures in Pt|Cu₂OSeO₃ heterostructures, *Phys. Rev. B* **94**, 134418 (2016).
- [12] H. Wang, D. Hou, Z. Qiu, T. Kikkawa, E. Saitoh, and X. Jin, Antiferromagnetic anisotropy determination by spin Hall magnetoresistance, *J. Appl. Phys.* **122**, 083907 (2017).
- [13] Y. Ji, J. Miao, Y. M. Zhu, K. K. Meng, X. G. Xu, J. K. Chen, Y. Wu, and Y. Jiang, Negative spin Hall magnetoresistance in antiferromagnetic Cr₂O₃/Ta bilayer at low temperature region, *Appl. Phys. Lett.* **112**, 232404 (2018).
- [14] L. Baldtrati, A. Ross, T. Niizeki, C. Schneider, R. Ramos, J. Cramer, O. Gomonay, M. Filianina, T. Savchenko, D. Heinze, A. Kleibert, E. Saitoh, J. Sinova, and M. Kläui, Full angular dependence of the spin Hall and ordinary magnetoresistance in

- epitaxial antiferromagnetic NiO(001)/Pt thin films, *Phys. Rev. B* **98**, 024422 (2018).
- [15] G. R. Hoogeboom, A. Aqeel, T. Kuschel, T. T. M. Palstra, and B. J. Van Wees, Negative spin Hall magnetoresistance of Pt on the bulk easy-plane antiferromagnet NiO, *Appl. Phys. Lett.* **111**, 052409 (2017).
- [16] J. Fischer, O. Gomonay, R. Schlitz, K. Ganzhorn, N. Vlietstra, M. Althammer, H. Huebl, M. Opel, R. Gross, S. T. B. Goennenwein, and S. Geprägs, Spin Hall magnetoresistance in antiferromagnet/heavy-metal heterostructures, *Phys. Rev. B* **97**, 014417 (2018).
- [17] J. Fischer, M. Althammer, N. Vlietstra, H. Huebl, S. T. B. Goennenwein, R. Gross, S. Geprägs, and M. Opel, Large Spin Hall Magnetoresistance in Antiferromagnetic α -Fe₂O₃/Pt Heterostructures, *Phys. Rev. Appl.* **13**, 014019 (2020).
- [18] Y. Cheng, S. Yu, M. Zhu, J. Hwang, and F. Yang, Electrical Switching of Tristate Antiferromagnetic Néel Order in α -Fe₂O₃ Epitaxial Films, *Phys. Rev. Lett.* **124**, 027202 (2020).
- [19] E. Cogulu, N. N. Statuto, Y. Cheng, F. Yang, R. V. Chopdekar, H. Ohldag, and A. D. Kent, Direct imaging of electrical switching of antiferromagnetic Néel order in α -Fe₂O₃ epitaxial films, *Phys. Rev. B* **103**, L100405 (2021).
- [20] I. Boventer, H. T. Simensen, A. Anane, M. Kläui, A. Brataas, and R. Lebrun, Room-Temperature Antiferromagnetic Resonance and Inverse Spin-Hall Voltage in Canted Antiferromagnets, *Phys. Rev. Lett.* **126**, 187201 (2021).
- [21] H. Wang, Y. Xiao, M. Guo, E. Lee-Wong, G. Q. Yan, R. Cheng, and C. R. Du, Spin Pumping of an Easy-Plane Antiferromagnet Enhanced by Dzyaloshinskii-Moriya Interaction, *Phys. Rev. Lett.* **127**, 117202 (2021).
- [22] R. Lebrun, A. Ross, O. Gomonay, V. Baltz, U. Ebels, A. L. Barra, A. Qaiumzadeh, A. Brataas, J. Sinova, and M. Kläui, Long-distance spin-transport across the Morin phase transition up to room temperature in ultra-low damping single crystals of the antiferromagnet α -Fe₂O₃, *Nat. Commun.* **11**, 6332 (2020).
- [23] A. Ross, R. Lebrun, M. Evers, A. Deák, L. Szunyogh, U. Nowak, and M. Kläui, Exceptional sign changes of the nonlocal spin Seebeck effect in antiferromagnetic hematite, *Phys. Rev. B* **103**, 224433 (2021).
- [24] Y. Cheng, S. Yu, A. S. Ahmed, M. Zhu, Y. Rao, M. Ghazisaeidi, J. Hwang, and F. Yang, Anisotropic magnetoresistance and nontrivial spin Hall magnetoresistance in Pt/ α -Fe₂O₃ bilayers, *Phys. Rev. B* **100**, 220408(R) (2019).
- [25] C. Schlueter, M. Lübke, A. M. Gigler, and W. Moritz, Growth of iron oxides on Ag (111)—reversible Fe₂O₃/Fe₃O₄ transformation, *Surf. Sci.* **605**, 1986 (2011).
- [26] K. Freindl, J. Wojas, N. Kwiatek, J. Korecki, and N. Spiridis, Reversible oxidation-reduction of epitaxial iron oxide films on Pt(111): Magnetite-hematite interconversion, *J. Chem. Phys.* **152**, 054701 (2020).
- [27] C. C. Chiang, S. Y. Huang, D. Qu, P. H. Wu, and C. L. Chien, Absence of Evidence of Electrical Switching of the Antiferromagnetic Néel Vector, *Phys. Rev. Lett.* **123**, 227203 (2019).
- [28] F. J. Morin, Magnetic susceptibility of α -Fe₂O₃ and α -Fe₂O₃ with added titanium, *Phys. Rev.* **78**, 819 (1950).
- [29] I. Dzyaloshinsky, A thermodynamic theory of “weak” ferromagnetism of antiferromagnetics, *J. Phys. Chem. Solids* **4**, 241 (1958).
- [30] J. O. Artman, J. C. Murphy, and S. Foner, Magnetic anisotropy in antiferromagnetic corundum-type sesquioxides, *Phys. Rev.* **138**, A912 (1965).
- [31] D. S. Ellis, E. Weschke, A. Kay, D. A. Grave, K. D. Malviya, H. Mor, F. M. F. De Groot, H. Dotan, and A. Rothschild, Magnetic states at the surface of α -Fe₂O₃ thin films doped with Ti, Zn, or Sn, *Phys. Rev. B* **96**, 094426 (2017).
- [32] N. Shimomura, S. P. Pati, Y. Sato, T. Nozaki, T. Shibata, K. Mibu, and M. Sahashi, Morin transition temperature in (0001)-oriented α -Fe₂O₃ thin film and effect of Ir doping, *J. Appl. Phys.* **117**, 17C736 (2015).
- [33] K. Mibu, K. Mikami, M. Tanaka, R. Masuda, Y. Yoda, and M. Seto, Thickness dependence of Morin transition temperature in iridium-doped hematite layers studied through nuclear resonant scattering, *Hyperfine Interact.* **238**, 92 (2017).
- [34] See Supplemental Material at <http://link.aps.org/supplemental/10.1103/PhysRevB.106.104419> for LEED patterns and STM images of Pt, magnetite, and hematite; details of CEMS measurements; and details of magnetotransport measurements.
- [35] http://ruff.geo.arizona.edu/AMS/xtal_data/DIFfiles/02426.txt.
- [36] R. E. Vandenberghe, C. A. Barrero, G. M. Da Costa, E. Van San, and E. De Grave, Mössbauer characterization of iron oxides and (oxy)hydroxides: The present state of the art, *Hyperfine Interact.* **126**, 247 (2000).
- [37] E. De Grave, R. M. Persoons, R. E. Vandenberghe, and P. M. A. De Bakker, Mössbauer study of the high-temperature phase of co-substituted magnetites, Co_xFe_{3-x}O₄ · I. $x \leq 0.04$, *Phys. Rev. B* **47**, 5881 (1993).
- [38] S. Gota, M. Gautier-Soyer, and M. Sacchi, Magnetic properties of Fe₂O₃ thin layers studied by soft x-ray linear dichroism, *Phys. Rev. B* **64**, 224407 (2001).
- [39] T. Hajiri, L. Baldrati, R. Lebrun, M. Filianina, A. Ross, N. Tanahashi, M. Kuroda, W. L. Gan, T. O. Menteş, F. Genuzio, A. Locatelli, H. Asano, and M. Kläui, Spin structure and spin Hall magnetoresistance of epitaxial thin films of the insulating non-collinear antiferromagnet SmFeO₃, *J. Phys.: Condens. Matter* **31**, 445804 (2019).
- [40] J. H. Han, C. Song, F. Li, Y. Y. Wang, G. Y. Wang, Q. H. Yang, and F. Pan, Antiferromagnet-controlled spin current transport in SrMnO₃/Pt hybrids, *Phys. Rev. B* **90**, 144431 (2014).
- [41] A. Barra, A. Ross, O. Gomonay, L. Baldrati, A. Chavez, R. Lebrun, J. D. Schneider, P. Shirazi, Q. Wang, J. Sinova, G. P. Carman, and M. Kläui, Effective strain manipulation of the antiferromagnetic state of polycrystalline NiO, *Appl. Phys. Lett.* **118**, 172408 (2021).
- [42] Y. Ji, J. Miao, K. K. Meng, X. G. Xu, J. K. Chen, Y. Wu, and Y. Jiang, Temperature dependence of spin Hall magnetoresistance in a Cr₂O₃ film with a TaO_x buffer layer, *Jpn. J. Appl. Phys.* **58**, 060911 (2019).
- [43] R. Lebrun, A. Ross, O. Gomonay, S. A. Bender, L. Baldrati, F. Kronast, A. Qaiumzadeh, J. Sinova, A. Brataas, R. A. Duine, and M. Kläui, Anisotropies and magnetic phase transitions in insulating antiferromagnets determined by a spin-Hall magnetoresistance probe, *Commun. Phys.* **2**, 50 (2019).
- [44] B. W. Dong, L. Baldrati, C. Schneider, T. Niizeki, R. Ramos, A. Ross, J. Cramer, E. Saitoh, and M. Kläui, Antiferromagnetic NiO thickness dependent sign of the spin Hall magnetoresistance in γ -Fe₂O₃/NiO/Pt epitaxial stacks, *Appl. Phys. Lett.* **114**, 102405 (2019).

- [45] X. Z. Chen, R. Zarzuela, J. Zhang, C. Song, X. F. Zhou, G. Y. Shi, F. Li, H. A. Zhou, W. J. Jiang, F. Pan, and Y. Tserkovnyak, Antidamping-Torque-Induced Switching in Biaxial Antiferromagnetic Insulators, *Phys. Rev. Lett.* **120**, 207204 (2018).
- [46] I. M. Miron, K. Garello, G. Gaudin, P. J. Zermatten, M. V. Costache, S. Auffret, S. Bandiera, B. Rodmacq, A. Schuhl, and P. Gambardella, Perpendicular switching of a single ferromagnetic layer induced by in-plane current injection, *Nature (London)* **476**, 189 (2011).
- [47] S. Łazarski, W. Skowroński, J. Kanak, Ł. Karwacki, S. Ziętek, K. Grochot, T. Stobiecki, and F. Stobiecki, Field-Free Spin-Orbit-Torque Switching in Co/Pt /Co Multilayer with Mixed Magnetic Anisotropies, *Phys. Rev. Appl.* **12**, 014006 (2019).